

# Tl<sub>4</sub>SnS<sub>3</sub>, Tl<sub>4</sub>SnSe<sub>3</sub> and Tl<sub>4</sub>SnTe<sub>3</sub> crystals as novel IR induced optoelectronic materials

I. Barchij<sup>1</sup> · M. Sabov<sup>1</sup> · A. M. El-Naggar<sup>4,5</sup> · N. S. AlZayed<sup>6</sup> · A. A. Albassam<sup>4</sup> · A. O. Fedorchuk<sup>2</sup> · I. V. Kityk<sup>3</sup>

Received: 15 October 2015 / Accepted: 16 December 2015 / Published online: 28 December 2015  
© The Author(s) 2015. This article is published with open access at Springerlink.com

**Abstract** A new type of chalcogenide crystals Tl<sub>4</sub>SnS<sub>3</sub>, Tl<sub>4</sub>SnSe<sub>3</sub>, Tl<sub>4</sub>SnTe<sub>3</sub> easily processing by external IR laser light is fabricated. For the titled crystals linear electrooptical effect was induced by external IR polarized light formed by two coherent beams of Er:glass nanosecond laser at fundamental wavelength 1540 nm. The detection of the electrooptical coefficient was performed by continuous-wave 1 W CO<sub>2</sub> laser at probing wavelength 10.6 μm. The origin of the effect is caused by an occurrence of the thin (up to 50 nm) photoexcited nanosheets which forms near the surface space charge density non-centrosymmetry. The relaxation of the electrooptics after switching off of the photoinduced Er:glass laser beam is explored for different types of samples at different power densities. The crystals may be used for IR optical triggering.

## 1 Introduction

Last years considerable efforts have been made for development of new infrared semiconductors used for operation in infrared spectral range [1, 2]. Particular interest present thallium chalcogenides [3, 4]. Up today several thallium containing chalcogenide ternary systems were studied. Among them Tl–Sn–S [5–7], Tl–Sn–Se [8–10] and Tl–Sn–Te [11–13]. Thallium and tin in their low oxidation state have a free doublet of electrons, which could create a stereochemical action and define mechanisms of carrier transport. In the low oxidation state the Tl<sub>4</sub>SnX<sub>3</sub> (X=S, Se, Te) type ternaries are formed in the relevant systems. All ternaries are crystallized in tetragonal 4/mmm crystallographic point group. Symmetry of Tl<sub>4</sub>SnS<sub>3</sub>(Se<sub>3</sub>) is tetragonal (space group P 4/nmm) [14, 15] and for Tl<sub>4</sub>SnTe<sub>3</sub> also is tetragonal (space group I 4/mcm) [16]. Generally they demonstrates also very promising IR induced properties [17] which do these materials very perspective for IR laser triggering.

The crystalline structure of Tl<sub>4</sub>SnSe<sub>3</sub> may be presented as a packing of some columns formed by Se octahedral surrounding Sn. The Tl atoms are located in voids between the longer columns. For the single crystals Tl<sub>4</sub>SnS<sub>3</sub>, Tl<sub>4</sub>SnSe<sub>3</sub> and Tl<sub>4</sub>SnTe<sub>3</sub> one can define cubes formed by cations with layers directed perpendicularly to the principal crystallographic axis (see Figs. 1, 2). In the space between the layers are situated isolated chalcogen atoms. Moreover, part of chalcogen atoms is located between cubes within the layers. In the case of the Tl<sub>4</sub>SnTe<sub>3</sub> chalcogen atoms are situated within the layers forming Te–Te pairs (Fig. 2) where tellurium atoms are located at a distance shorter than the sum of ionic radii for the each Te.

Although the inter-atomic distance within cubes of atoms cations (Fig. 3) (following the structural data [5–7]) are outside the sum of ionic radii of the respective atoms

✉ I. V. Kityk  
iwank74@gmail.com

<sup>1</sup> Chemical Department, Uszgorod University, Uzhgorod, Ukraine

<sup>2</sup> Department of Inorganic and Organic Chemistry, Lviv National University of Veterinary Medicine and Biotechnologies, Pekarska St. 50, Lviv 79010, Ukraine

<sup>3</sup> Faculty of Electrical Engineering, Czestochowa University Technology, Armii Krajowej 17, 42201 Czestochowa, Poland

<sup>4</sup> Research chair of Exploitation of Renewable Energy Applications in Saudi Arabia, Physics and Astronomy Department, College of Science, King Saud University, P.O. Box 2455, Riyadh 11451, Saudi Arabia

<sup>5</sup> Physics Department, Faculty of Science, Ain Shams University, Abassia, Cairo 11566, Egypt

<sup>6</sup> Physics and Astronomy Department, College of Science, King Saud University, P.O. Box 2455, Riyadh 11451, Saudi Arabia

**Fig. 1** Laying clusters of atoms in the structure of crystalline compounds  $Tl_4SnS_3$  and  $Tl_4SnSe_3$

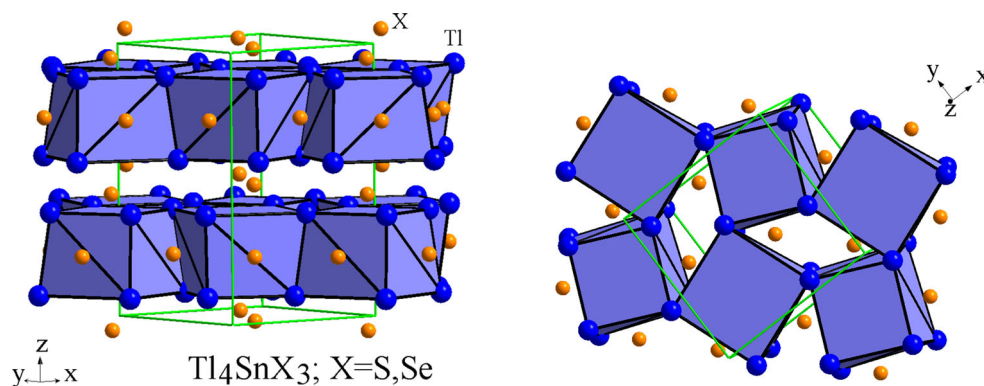


**Fig. 2** Laying clusters of atoms and cation pairs in Te–Te compound structure  $Tl_4SnTe_3$

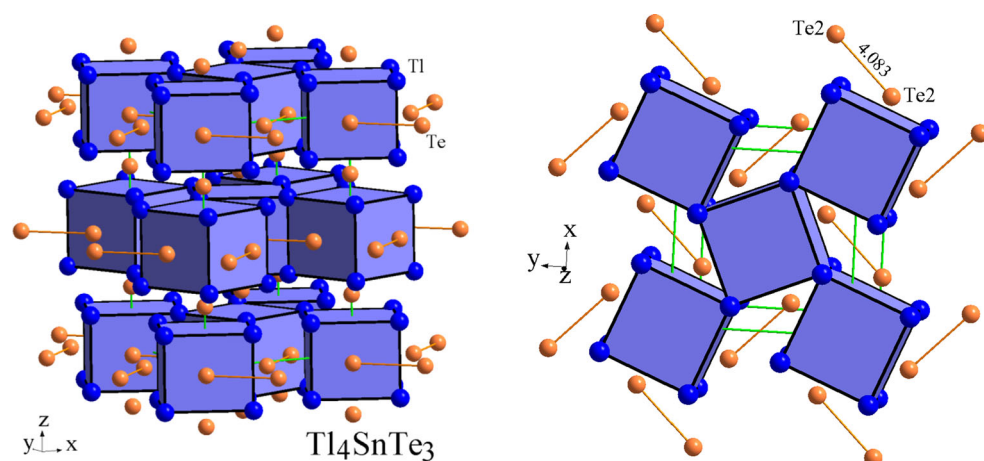
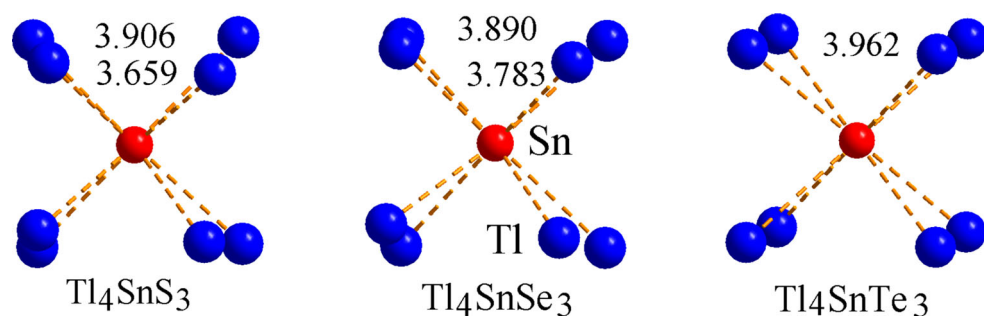


**Fig. 3** Inter-atomic distances Tl–Sn for the studied compounds



such clusters (cubes) are formed by positively charged atoms and individual cation or anion pairs of atoms. The later form a ground state dipole moments with magnitudes higher than 5 D. Such magnitudes of ground dipole moments can manifest itself interesting piezoelectric and photoinduced nonlinear optical features.

## 2 Experimental

The ternaries synthesized from the elements of high purity (Tl–99.99 wt%, Sn–99.998 wt%, S–99.999 wt%, Se–99.999 wt%, Te–99.99 wt%). The crystals were grown by

Bridgman method. The thallium was covered by oxide in a surface, which was removed before using. All synthesis was carried out in previously cleaned and dried quartz tubes with narrow end. Then, they were vacuum-sealed (0.13 Pa). According to  $Tl_2X-SnX$  (X–S, Se, Te) phase diagrams  $Tl_4SnSe_3(Te_3)$  melt congruently, but  $Tl_4SnS_3$ —incongruently. Given this factor  $Tl_4SnSe_3(Te_3)$  were synthesized from stoichiometric amounts of components and  $Tl_4SnS_3$ —from non-stoichiometric content which is richer by SnS originating from the region of primary crystallization of the ternary compound. The samples were heated to liquid state (673 K for  $Tl_4SnS_3$ , 763 for  $Tl_4SnSe_3$  and 873 K for  $Tl_4SnTe_3$ ). They were hold for 24 h at maximal

temperature. Then it was subjected to a cooling until the annealing temperature (453 K for  $\text{Tl}_4\text{SnS}_3$ , 523 K for  $\text{Tl}_4\text{SnSe}_3$  and 583 K for  $\text{Tl}_4\text{SnTe}_3$ ) and maintained during 3 days. Then the samples were placed into vertical two zone furnace. The temperatures of the zones were maintained with  $\pm 0.5$  K accuracy. The solidification rate was 0.1–0.3 mm/h, and the temperature gradient at the solid–liquid interface was 2–4 K/mm. The temperatures of the solidification zone were fixed to annealing temperature.

The monitoring of the Pockels effects was performed by continuous wave (cw) 10.6  $\mu\text{m}$   $\text{CO}_2$  laser with power about 1 W. The ZnSe polarizer was used for the Senarmont procedure to evaluate birefringence [18] in order to detect changes of the birefringence under applied pulsed dc-electric field with frequency repetition about 50 kHz and amplitude up to 10 kV/cm. The probing  $\text{CO}_2$  laser beam was temporary synchronized with the external pulsed dc-electric rectangular pulses. The accuracy of birefringence measurements was about  $10^{-5}$  which allowed to evaluate the Pockels effective electrooptics effect (EOE) coefficient with accuracy up to 0.02 pm/V. 15 ns Er:glass laser with pulse duration up to 1  $\text{GW}/\text{cm}^2$  splitted on to coherent beams was used as photoinduced processing laser breaking the centrosymmetry in the two-beam geometry. The set-up allowed to vary the incident angles of the photoinduced laser with respect to the sample surfaces. Different crystallographic planes of the titled crystals were examined.

The titled crystals had the surfaces with sizes about 2–3 mm. The surface's roughness was about 12  $\mu\text{m}$ .

### 3 Results and discussion

Our spectroscopy studies have shown that the energy gap for the titled  $\text{Tl}_4\text{SnS}_3$ ,  $\text{Tl}_4\text{SnSe}_3$ ,  $\text{Tl}_4\text{SnTe}_3$  single crystals have been varied within 0.2–0.6 eV. Our main goal was to process these crystals in order to excite a thin layer near the surface (up to 30 nm). As a consequence we form a thin photoexcited layer (up 50 nm) with non-centrosymmetric charge density distribution which in turn is substantially different with respect to the bulk state being centro-symmetric. Appearance of this photoexcited level is a main source of occurrence the effects described by third rank polar tensors requiring charge density acentricity. This may be of particular interest for the IR operated electrooptical devices.

So we have excited the samples above the energy gap using  $\text{Er}^{3+}$ :glass laser wavelength 1.54  $\mu\text{m}$ . As a consequence the single near-the interface layer with sheet thickness up to 50 nm was served as a source of the photo induced Pockels effect.

The typical computer reconstructed images of the electrooptical birefringence beam profile sequence in crossed polarizers are presented in the Figs. 4, 5, 6 and 7 for several

photoinduced power densities. We have used the different polished crystallographic planes of the studied crystals and the effect has demonstrated a slight dependence on anisotropy. The maximal changes were achieved during incident angle of the photoinduced laser varying within  $20^\circ$ – $25^\circ$  with respect to the surface for the two splitted beams. S-polarization of the photoinduced beam was preferred. The probing 1 W cw  $\text{CO}_2$  laser was incident normally to the surfaces of the samples.

In the Fig. 4 is presented the computationally simulated image profile for space distribution of  $\text{CO}_2$  probing laser beam after passing the  $\text{Tl}_4\text{SnS}_3$  single crystals and crossed polarizers during simultaneous superposition of the photoinduced power density (about  $200 \text{ MW}/\text{cm}^2$ ) and the pulsed dc-electric field with electric strength about 10 kV/cm at 50 kHz. The image is done in the cross polarized regime and was reconstructed by PC. The effect is clearly seen and it disappears after several seconds after switching off of the laser and dc-electric treatment.

During the performance of processing of a crystal possessing different anion—(Se) (see Fig. 5) one can see substantially different space distribution of the propagated light. Additionally there occur additional lines corresponding to formation of some space gratings under influence of the infrared light due to IR induced nonlinearities [19, 20]. Moreover, there occurs some scattering due to presence of some macroscopical inclusions, however its background to the output signal did not exceed 2.3 %. The shape of the

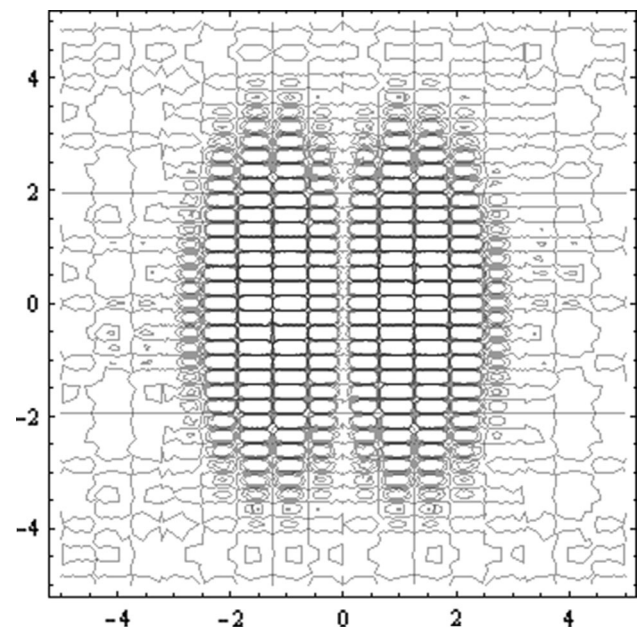


**Fig. 4** Typical photoinduced optical anisotropy sequence under influence photoinduced EOE effect at two-beam photoinduced Er:glass power density equal to about  $200 \text{ MW}/\text{cm}^2$  for applied dc-electric strength about 10 kV/cm at 50 kHz for  $\text{Tl}_4\text{SnS}_3$ . The achieved output effective EOE magnitude was equal to 0.08 pm/V. The picture was reconstructed using a statistics over the 2000 pulses. The scale is given in mm



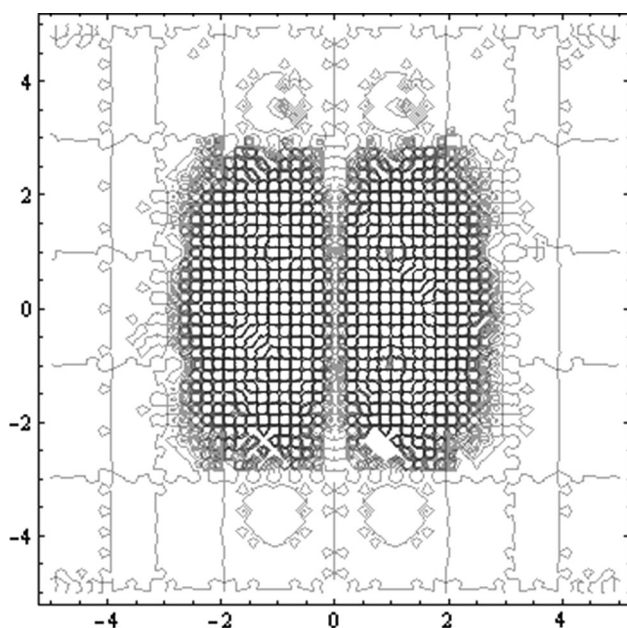


**Fig. 5** The same as previously for the  $200 \text{ MW/cm}^2$  for the  $\text{Ti}_4\text{SnSe}_3$ . Effective EOE coefficient was equal to  $0.13 \text{ pm/V}$ . All the scales are in mm

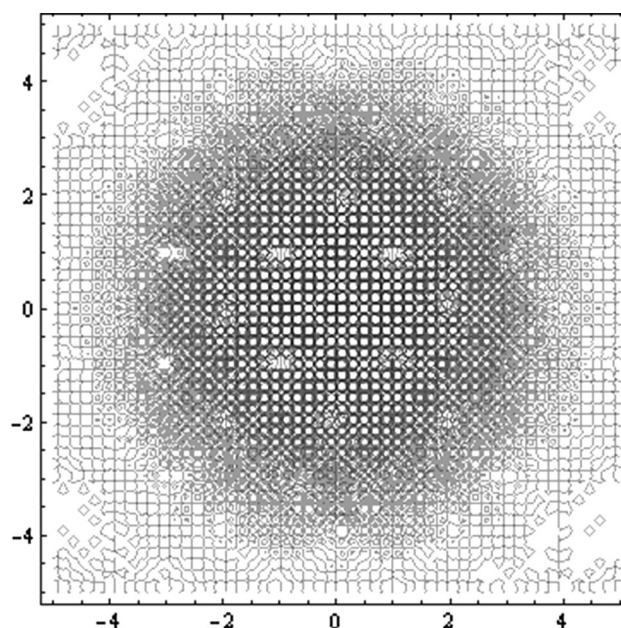


**Fig. 7** The same as in the three previous cases for power density about  $1 \text{ GW/cm}^2$  for  $\text{Ti}_4\text{SnTe}_3$ . Effective EOE coefficient was equal to  $0.24 \text{ pm/V}$

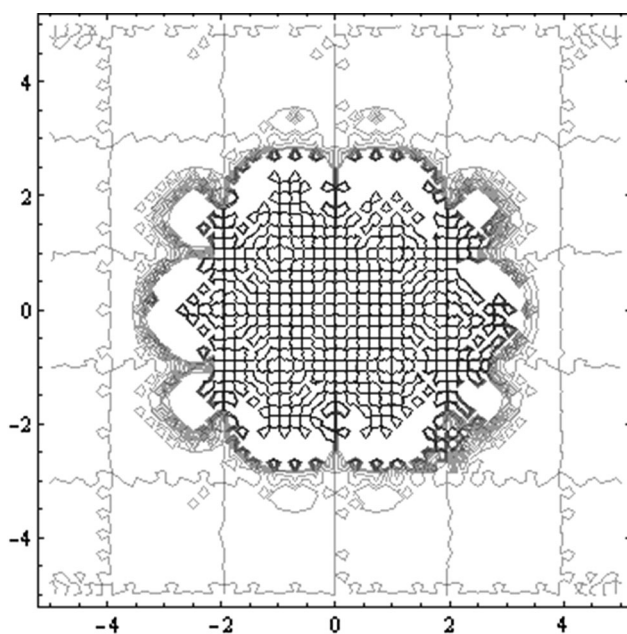


**Fig. 6** The image of the beam sequence for the probing beam at photoinduced power density  $0.7 \text{ GW/cm}^2$  for the  $\text{Ti}_4\text{SnTe}_3$ . Effective EOE tensor coefficient was equal to  $0.27 \text{ pm/V}$  at  $10.6 \mu\text{m}$

lines reflects a non-Gaussian profile of the excited IR laser lines which is substantially deformed due to some multiphoton processes [21, 22]. The maximally achieved magnitude was equal to about  $0.12 \text{ pm/V}$ .

With the further undergoing to anions with higher polarizabilities (Te) (see Fig. 6) and varied power densities

there occurs a substantial changes of the beam profile shapes propagating through the samples. Such profile diameter has lost their prolonged structure and was substantially less. At the same time the observed photoinduced EOE coefficient ( $0.27 \text{ pm/V}$ ) is several times higher than for the two previous cases. This fact confirms a principal role for the penetrated photoinduced light length and the photoinduced polarizability which for the case of the Te compounds will be higher. The effect is optimal for the S-light polarization, however the anisotropy of different planes of the crystals do not influence substantially on the output.

The further enhancement of the power density leads to occurrence of more radial structure of the photoinduced EOE and the space distribution is more homogenous. Additionally the value of the EOE was maximal ( $0.24 \text{ pm/V}$ ). One can expect that substantial role could also play here photoinduced lattice phonons and especially anharmonic ones [23].

Generally the presented results show that the maximal photoinduced electrooptics is observed for the Te containing samples and correlates well with the minimal energy gap and maximal ground state dipole moments defining the polarizability. The optimal EOE is achieved for the power density varying within  $0.2\text{--}0.5 \text{ GW/cm}^2$ . The further power increase leads to a some suppression of the effect. The effect disappeared after switching off of the photoinduced beam power during to several seconds. The

optimal polarization of the laser beams for this case was S-type. Undergoing to P or SP polarizations has given decrease of the electrooptics efficiency up to 50 %. The incident angles were varied within the 24°–28° with respect to the surfaces. The obtained results show that the use of the such crystals may be commensurable or even better than for traditional chalcogenide photonics materials [24, 25] which is caused by a presence of heavy cations. Additionally these materials may be applied as electric field operated gratings in the IR spectral range complementary to organic gratings materials [26]. The effect may be commensurable with the similar effects for the TI containing chalcogenides [27]. The beam profile of the CO<sub>2</sub> laser was deviated from Gaussian from 15 up to 30 % and its influence on the results was <0.5 %.

#### 4 Conclusions

We have found an occurrence of the optically induced transparency during study of Pockels effect at 10.6 μm laser probing wavelength. The photoinduction was carried out by two coherent splitted nanosecond Er:glass laser at 1540 nm with power density varying from 0.1 up to 1 GW/cm<sup>2</sup>. This effect is originated from a thin near the surface nanosheets formed by photoinduced treatment. The detection of the EO effect was performed for the 10.6 μm cw CO<sub>2</sub> laser probing beam with power about 1 W. The maximally achieved EOE coefficient at 10.6 μm was equal to 0.24 pm/V. The EOE was maximal for Te containing samples and this maximum correlates well with the minimum of energy gap and maximal ground state dipole moments. The effect is completely reversible after switching off the IR induced treatment and dc-electric field. The materials may be used for fabrication of IR induced electrooptically operated gratings

**Acknowledgments** The project was financially supported by King Saud University, Vice Deanship of research chairs.

**Compliance with ethical standards**

**Conflict of interests** None.

**Open Access** This article is distributed under the terms of the Creative Commons Attribution 4.0 International License (<http://creativecommons.org/licenses/by/4.0/>), which permits unrestricted use, distribution, and reproduction in any medium, provided you give appropriate credit to the original author(s) and the source, provide a link to the Creative Commons license, and indicate if changes were made.

#### References

1. M. Piasecki, G. Lakshminarayana, A.O. Fedorchuk, O.S. Kushnir, V.A. Franiv, A.V. Franiv, G. Myronchuk, K.J. Plucinski, J. Mater. Sci. Mater. Electron. **24**, 1187–1193 (2013)
2. V.R. Kozler, V.V. Bozhko, O.V. Parasyuk, O.V. Novosad, A.O. Fedorchuk, J. Mater. Sci. Mater. Electron. **25**, 163–167 (2014)
3. B.A. Kuropatwa, A. Assoud, H. Kleinke, J. Alloy. Compd. **509**, 6768–6772 (2011)
4. A. Kosuga, K. Kurosaki, H. Muta, S. Yamanaka, J. Appl. Phys. **99**, 063705 (2006)
5. A.L. Ajavon, R. Eholie, Y. Piffard, M. Tournoux, Rev. Chim. Miner. **20**, 421–425 (1983)
6. A. Ibanez, J.C. Jumas, E. Philippot, A.L. Ajavo, R. Eholie, Rev. Chim. Miner. **23**, 281–289 (1986)
7. T.A. Malakhovskaya-Rosokha, M.Y. Sabov, I.E. Barchiy, E.Y. Peresh, Russ. J. Inorg. Chem. **56**, 118 (2011)
8. P. Houenou, R. Eholie, J. Flahaut, C. R. Acad. Sci. Paris **283C**, 193–195 (1979)
9. P. Houenou, R. Eholie, J. Flahaut, J. Less Common Met. **81**, 181–197 (1981)
10. P. Houenou, A.L. Ajavon, G.A. Fatseas, C. R. Acad. Sci. Paris **295**, 455–457 (1982)
11. E. Dichi, G. Kra, R. Eholie, B. Legendre, J. Alloys Compd. **194**, 155–161 (1993)
12. E. Dichi, G. Kra, R. Eholie, B. Legendre, J. Alloys Compd. **199**, 7–19 (1993)
13. E. Dichi, G. Kra, R. Eholie, B. Legendre, J. Alloys Compd. **199**, 21–46 (1993)
14. S. Bucchia, C. Jumas, E. Philippot, M. Maurin, Revue de Chimie Minerale **18**, 224–234 (1981)
15. S. Bradtmöller, R.K. Kremer, P. Böttcher, Z. Anorg. Allg. Chem. **620**, 1073–1080 (1994)
16. S. Bradtmöller, P. Böttcher, Z. Anorg. Allg. Chem. **619**, 1155–1160 (1993)
17. H. Reshak Ali, K. Plucinski, M.J. Filep, M.Y. Sabov, I. Barchij, A.O. Fedorchuk, M. Kowar-Pokladko, Z.A. Alahmed, H. Kamarudin, Int. J. Electrochem. Sci. **9**, 6068–6073 (2014)
18. Toru Yoshizawa (ed.), *Handbook of Optical Metrology: Principles and Applications*, 2nd edn. (Wiley, London, 2015)
19. W. Gruhn, Opt. Appl. **42**, 467–472 (2012)
20. P. Tsoi, N. Gololobov, Opt. Appl. **43**, 353–358 (2013)
21. E. Nicoletti, G. Zhou, B. Jia, M.J. Ventura, D. Bulla, B. Luther-Davies, M. Gu, Opt. Lett. **33**, 2311–2313 (2008)
22. M.A. Foster, A.C. Turner, M. Lipson, A.L. Gaeta, Opt. Express **16**, 1300–1320 (2008)
23. O. Delaire, J. Ma, K. Marty, A.F. May, M.A. McGuire, M.-H. Du, D.J. Singh, A. Podlesnyak, G. Ehlers, M.D. Lumsden, B.C. Sales, Nat. Mater. **10**, 614–619 (2011)
24. H. Fritzsche, in *Light Induced Structural Changes in Glasses, in Insulating and Semiconducting Glasses*, ed. by P. Boolchand (World Scientific, Singapore, 2000), pp. 653–690
25. S. Wong, M. Deubel, F. Perez-Willard, S. John, G.A. Ozin, Adv. Mat. **18**, 265–269 (2006)
26. M.R. Beaulieu, N.R. Hendricks, J.J. Watkins, ACS Photonics **1**, 799–805 (2014)
27. N.S. AlZayed, J. Ebothé, J. Michel, I.V. Kityk, A.O. Fedorchuk, O.V. Parasyuk, G. Myronchuk, Phys. E **65**, 130–181 (2015)